

Three-Dimensional Distribution of the ISM in the Milky Way Galaxy: II. The Molecular Gas Disk

Hiroyuki NAKANISHI¹ and Yoshiaki SOFUE²

¹*Nobeyama Radio Observatory, Minamimaki, Minamisaku, Nagano 384-1305*

²*Institute of Astronomy, The University of Tokyo, 2-21-1 Osawa, Mitaka, Tokyo 181-0015*
hnakanis@nro.nao.ac.jp

(Received 2006 February 14; accepted 2006 August 3)

Abstract

We created a three-dimensional distribution map of molecular gas throughout the Milky Way Galaxy using the latest $^{12}\text{CO}(J=1-0)$ survey data cube and rotation curve based on the kinematic distance. The radial distribution of the molecular gas shows a central peak and a second peak around $0.5 R_0$. The thickness of the molecular disk slightly increases from 48 pc to 160 pc with the galactocentric distance within a radius range of 0–11 kpc. We were able to trace the Outer, the Perseus, the Sagittarius-Carina, the Scutum-Crux, and the Norma arms as logarithmic spiral arms with pitch angles of $11^\circ - 15^\circ$. Considering that the pitch angles of the spiral arms are within this range, the Norma and the Outer arms seem to be identified as the same spiral arm. We could also trace a midplane displacement, whose amplitude is nearly constant inside a 10 kpc radius and increases beyond this radius. The ridges of midplane displacement form leading spiral arms.

Key words: Galaxy: disk — Galaxy: kinematics and dynamics — Galaxy: structure — ISM: kinematics and dynamics — radio lines: ISM

1. Introduction

The global three-dimensional (3D) structure of the Milky Way Galaxy is one of the essential informations to study the Galactic objects in detail. In Paper I (Nakanishi & Sofue 2003), we have analyzed the latest 21-cm line survey data, and presented the 3D distribution map of H I gas in the Milky Way Galaxy. In this paper, we deal with the molecular gas distribution as Part II of this series.

A survey in the $^{12}\text{CO}(J=1-0)$ line is a good tool for tracing the interstellar matter (ISM) in the inner disk of the Milky Way Galaxy (inside the solar orbit), while the H I data is advantageous for study of ISM in the outer disk (outside the solar orbit). One of the most famous CO line surveys is the Columbia CO survey, whose earlier survey was carried out with the 1.2-m telescopes in New York City, USA, and Cerro Tololo, Chile (Dame et al. 1987; Bronfman et al. 1988; Bronfman et al. 1989). This survey covered the entire Milky Way with a grid spacing of 0.5° . Another higher resolution survey is the Massachusetts–Stony Brook Galactic plane CO survey, which was made using the 14-m telescope of the Five College Radio Astronomy Observatory (FCRAO) (Sanders et al. 1986). The covered ranges of the galactic longitude and latitude were from $l = 8^\circ$ to 90° and from $b = -1.05^\circ$ to $+1.05^\circ$ in the first quadrant, respectively. The grid spacing was $3' \times 3'$ or $6' \times 6'$. These large CO surveys were ideal for exploring into the molecular gas distribution in the Milky Way Galaxy. There have been several studies on the Galactic structure using these data.

Dame et al. (1986) and Myers et al. (1986) showed face-on views of the first Galactic quadrant examining positions of the largest individual molecular complexes identified in the Columbia CO survey of the first Galactic quadrant (Cohen, Dame, & Thaddeus 1986). They found clear evidence for the

Sagittarius spiral arm. Cohen et al. (1985), Grabelsky et al. (1987), and Grabelsky et al. (1988) showed distribution of giant molecular clouds in the fourth quadrant and they clearly delineated the Carina arm. Clemens, Sanders, & Scoville (1988) presented the molecular gas distribution in the first quadrant of the inner disk of the Milky Way Galaxy using the Massachusetts–Stoneybrook CO survey, found a ring-like structure at the radius of $0.5 R_0$ (R_0 : the Galactocentric distance of the Sun), and traced the Sagittarius and Perseus arms. The distance of the molecular gas was determined by the kinematic distance using a rotation curve. The near–far problem in the inner Galaxy was overcome by introducing a vertical model of the molecular gas distribution. Solomon & Rivolo (1989) showed a face-on view of the Milky Way Galaxy examining individual giant molecular clouds identified in the Massachusetts–Stoneybrook CO survey.

Hunter et al. (1997) presented the molecular gas distributions in the entire Galactic disk of the Milky Way Galaxy using the Columbia survey (Dame et al. 1987) for modeling the diffuse gamma-ray emission. The distance of the molecular gas was determined by the kinematic distance. Although there is a near–far problem in the inner disk, they **divided** gas density equally at near and far points for $b = 0^\circ$.

Sawada et al. (2004) determined the molecular gas distribution in the Galactic center by considering the absorption of the OH line to determine the line-of-sight distance of the molecular gas, using the CO data cube of Bitran et al. (1997). They found that molecular gas is elongated in the line-of-sight direction against the Sun, and that this feature is associated with a central galactic bar.

Thus, there are several studies on the molecular gas distribution. However, there has been no three-dimensional gas density map of the whole Galaxy. Dame, Hartmann, & Thaddeus

(2001) published a new compilation of Columbia $^{12}\text{CO}(J=1-0)$ survey of the whole of the Milky Way Galaxy. The sampling and the sensitivity of this survey were much improved over that of the old Columbia survey. This is a great tool for investigating the molecular gas distribution throughout the entire Milky Way Galaxy. In this paper, we show a molecular gas distribution in the Milky Way Galaxy using the Columbia $^{12}\text{CO}(J=1-0)$ survey data and the latest rotation curve.

2. DATA

We used the latest compilation of $^{12}\text{CO}(J=1-0)$ survey data (Dame, Hartmann, & Thaddeus 2001), which were obtained with the 1.2-m telescopes in New York City, USA, and Cerro Tololo, Chile. The half-power beam width (HPBW) was $8''.4$, which corresponded to 2.4 pc at the heliocentric distance of 1 kpc. The data consisted of $^{12}\text{CO}(J=1-0)$ line spectra over the entire Milky Way. We used data of surveys named 2, 8, 18, 31, 33, and 36. Grid spacing of these data was $0^\circ.125 - 0^\circ.25$. The total radial velocity (V_r) coverage was 332 km s^{-1} and velocity resolution was 1.3 km s^{-1} . The r.m.s. noise level per channel was $0.12 - 0.43 \text{ K}$. We used spectra within a Galactic latitude range of $|b| \leq 1.5^\circ$.

The rotation curve, which we used to transform the radial velocity of the CO gas into the distance, is the same as we used in Paper I. The inner and outer rotation curves are taken from Clemens (1985) and Dehnen and Binney (1998), respectively. The Galactic constants $R_0 = 8.0 \text{ kpc}$ (the Galactocentric distance of the Sun) and $V_0 = 217 \text{ km s}^{-1}$ (the solar rotational velocity) are adopted.

3. METHOD

3.1. Binding the Data

3.1.1. Inner Galaxy

For the inner Galaxy, we averaged the CO data over five channels ($\geq 6.5 \text{ km s}^{-1}$ velocity width) for each spectrum in order to eliminate the cloud-cloud motion of $3 - 3.9 \text{ km s}^{-1}$ (Clemens 1985; Alvarez et al. 1990) and to obtain a higher signal-to-noise ratio (S/N ratio).

The molecular gas is distributed in a more clumpy form than the H I gas. Since we intend to develop our understanding of the global structure of the Milky Way Galaxy, we must smooth the CO emission on a larger scale in order to eliminate such a clumpy features and to model the vertical structure of the molecular gas disk. Since the typical scale of the random motion of the molecular clouds is $0.015 R_0 \text{ kpc}$ (Clemens 1985), we averaged the data over a 240 pc width when the line-of-sight length corresponding to 6.5 km s^{-1} velocity width was smaller than 240 pc. Thus the CO data were averaged over $\geq 6.5 \text{ km s}^{-1}$ velocity width and $\geq 240 \text{ pc}$ width.

In addition, we averaged the data in the longitudinal direction to eliminate the clumpy features of CO clouds and to obtain a much higher S/N ratio. For the first ($0^\circ \leq l \leq 90^\circ$) and fourth ($270^\circ \leq l \leq 360^\circ$) quadrants, we bound the data, so that the longitudinal width at the tangential point is equal to 240 pc-width.

Thus the CO data were averaged over $\geq 240 \text{ pc}$ in the line-of-sight direction and longitudinal direction except for the inner

region of the tangential radius, where the data were averaged over $\geq 240 \text{ pc}$ width only in the line-of-sight direction. The data were not averaged in the latitudinal direction at all.

3.1.2. Outer Galaxy

For the outer Galaxy, we averaged the data in the longitudinal direction so that longitudinal separation becomes $0''.5$, which is nearly the same as the H I data. Moreover, we averaged the CO data over two channels ($\geq 2.6 \text{ km s}^{-1}$ velocity width), which is also the same as the H I data.

Figure 1 shows the points where the molecular gas densities were calculated.

3.2. Molecular Gas Distribution in the Outer Galaxy

In this paper, we choose a Cartesian coordinate whose x -axis coincides with the line crossing the Sun and the Galactic center and whose origin coincides with the Galactic center. The z -axis is chosen so that it is parallel to the rotational axis. The Sun is located at $(-8 \text{ kpc}, 0, 0)$. We also choose a cylindrical coordinate (R, θ, z) so that the angle $\theta = 180^\circ$ coincides with the direction toward the Sun and the angle $\theta = 90^\circ$ is parallel to $l = 90^\circ$.

The distance of the molecular gas was determined by kinematic distance in this paper, the same way as in Paper I. The distance of molecular gas in the outer disk ($R > R_0$) is uniquely determined, and then we obtained the molecular gas distribution in the outer disk using the equation

$$n_{\text{H}_2} = X T_b \frac{\Delta V_r}{\Delta r} \quad (1)$$

where n_{H_2} denotes the volume number density of the molecular hydrogen H_2 , X the CO-to- H_2 conversion factor, and r the heliocentric distance. We adopted two kinds of conversion factor; (1) a constant conversion factor of $X = 1.8 \times 10^{20} (\text{H}_2 \text{ cm}^{-2} \text{ K}^{-1} \text{ km}^{-1} \text{ s})$ (Dame, Hartmann, & Thaddeus 2001) and (2) a varying conversion factor with the Galactocentric distance (Arimoto, Sofue, & Tsujimoto 1996). Arimoto, Sofue, & Tsujimoto (1996) calculated X using the data in Solomon et al. (1987).

Since the conversion factor can be approximately expressed by exponential function of the Galactocentric radius, we fitted an exponential function to the resultant radial profile and obtained the following equation,

$$X [\text{H}_2 \text{ cm}^{-2} \text{ K}^{-1} \text{ km}^{-1} \text{ s}] = 1.4 \exp(R/11 \text{ kpc}). \quad (2)$$

3.3. Molecular Gas Distribution in the Inner Galaxy

There is, on the other hand, a near-far ambiguity in the inner disk ($R < R_0$); i.e. there are two heliocentric distances satisfying the same radial velocity. Therefore, we could not determine the H_2 distribution in the inner Galaxy in the same way as in the outer Galaxy. In order to divide molecular distributions at near and far points, we introduced the vertical structure of the Galactic disk. Following Spitzer (1942), we assumed that the vertical distribution of the molecular gas is expressed with

$$n(z) = n_0 \text{sech}^2(\xi), \quad (3)$$

$$\xi = \log(1 + \sqrt{2}) \frac{z - z_0}{z_{1/2}}, \quad (4)$$

where z and $z_{1/2}$ denote the height from the Galactic plane ($b = 0^\circ$) and the scale-height, respectively. At $z = z_{1/2}$ the density, n , gets a half value of the maximum at the midplane. The subscript 0 means values at the midplane. The scale-height was determined at the tangential points in the inner Galaxy, which is described in the next subsection.

Assuming that the vertical distribution of the H_2 gas follows equation (3), the H_2 column density, $N_{H_2}(b)$, is represented as a function of the Galactic latitude b using four parameters: n_{H_21} , n_{H_22} , z_{01} , and z_{02} . That is,

$$N_{H_2}(b) = n_{H_21} \text{sech}^2(\xi_1) \frac{\Delta r_1}{\cos b} + n_{H_22} \text{sech}^2(\xi_2) \frac{\Delta r_2}{\cos b}, \quad (5)$$

where

$$\xi_1 = \log(1 + \sqrt{2}) \frac{r_1 \tan b - z_{01}}{z_{1/2}}, \quad (6)$$

$$\xi_2 = \log(1 + \sqrt{2}) \frac{r_2 \tan b - z_{02}}{z_{1/2}}. \quad (7)$$

For each point shown in figure 1, we sought a parameter set consisting of n_{H_21} , n_{H_22} , z_{01} , and z_{02} , which gives the smallest residual in subtracting the model distribution from the observation. The fitting resolution of the four parameters is $0.01 H_2 \text{ cm}^{-3}$ for n_{H_21} and n_{H_22} , and 1 pc for z_{01} and z_{02} , respectively. We restricted z_{01} and z_{02} within a range of -250 pc to $+250$ pc. The grid spacing is 0.125° , which corresponds < 17 pc at tangential points, at most points in the inner Galaxy. Since there are enough points (more than three points) to resolve near vertical distribution, it is possible to divide the total CO emission into near and far emissions. We thus obtained parameter sets of n_{H_21} , n_{H_22} , z_{01} , and z_{02} for discrete points in the inner Galaxy.

To show how well the fitting method works, we present a residual map in figure 2. In order to make this map, we first measured standard deviation of residuals between a fitted model curve and observed data. And then, we calculated relative residuals, which is a fraction of the standard deviation relative to the peak of the observational data. This residual map shows that the relative residual is less than 20 – 30 % in most of the region, and that the fitting method does not work well near the Sun.

3.4. Scale-height

Tangential points which satisfy $R = R_0 \sin l$ present no near-far problem in the inner Galaxy. Hence, the vertical structure at the tangential points can be determined uniquely.

The gas of velocity range $|V_{r,\max} - \sigma| < |V_r| < \infty$ is located at the tangential points, where V_r , $V_{r,\max}$, and σ are radial velocity, maximum radial velocity, and random velocity, respectively. The random velocity was taken to be 5 km s^{-1} (Clemens 1985). We thus obtained vertical distributions, and fitted a model distribution $\rho(z) = \rho_0 \text{sech}^2(\xi)$ to determine a scale-height of $z_{1/2}$. Figure 3 shows a full-width half maximum (FWHM) ($2z_{1/2}$) plotted versus the Galactocentric radius, which is a mean value in a 1 kpc bin. For a comparison, figure 3 shows also FWHM of molecular disk calculated by Bronfman et al. (1988) and Grabelsky et al. (1987), who use the same data that we use. We adopt the Galactic constant R_0 of 8 kpc although Bronfman et al. (1988) and Grabelsky et al.

(1987) use R_0 of 10 kpc. Therefore, the radius and FWHM are reduced by factor of 8/10. Filled squares, open circles, and open triangles denote the data from this study, Bronfman et al. (1988) and Grabelsky et al. (1987), respectively. Our result is almost consistent with Bronfman et al. (1988) and Grabelsky et al. (1987).

Figure 4 shows comparisons of a model and observations. A vertical distributions of molecular gas can be approximately reproduced by equation (3).

— Figure 3 —

3.5. Construction of Three-Dimensional Map

We thus obtained parameter sets of the molecular distribution at each point of figure 1.

First, the parameter sets obtained for the discrete points in the inner Galaxy were averaged with a Gaussian function whose FWHM is 0.48 kpc, in order to eliminate data with bad fitting results. Then we calculated the H_2 distribution in the inner Galaxy using the averaged parameter sets. The H_2 gas densities obtained at the discrete points in the outer Galaxy were transformed into continuous distribution by interpolating with the same Gaussian function. Averaging length for the z -direction was fixed at 35 pc, which corresponds to the grid spacing of 0.25° at the heliocentric distance of 16 kpc. Finally, we combined the H_2 distributions in the inner and outer Galaxy to obtain a CO distribution cube. In this paper, the grid spacing of the cube is fixed at 200 pc for the x and y directions and at 20 pc for the z directions, and the size of the resultant cube is $40 \text{ kpc} \times 40 \text{ kpc} \times 2 \text{ kpc}$ in x , y , and z direction, respectively.

Since the number of points where the molecular gas densities were calculated (figure 1) in the azimuthal range $|\theta| < 30^\circ$ is too few to make a map, we do not show this region.

— Figure 1 —

4. Results

4.1. A Face-on Map

Figure 5 shows a face-on map of the molecular H_2 gas in the Milky Way Galaxy.

Figure 6 shows a face-on map of the molecular gas when the conversion factor is calculated with equation (2). In this map, the molecular gas distribution in the outer region is slightly enhanced. However, there is no large difference between these maps. Hence, our discussions below about the structure of the molecular gas distribution are based on the H_2 map obtained adopting a constant conversion factor for simplicity.

— Figure 5 —

— Figure 6 —

— Figure 14 —

4.2. Vertical Sliced Maps

Figures 7 and 8 present vertical cross sections of the resultant cube sliced with planes which are parallel to the z -axis. We made 6 slices at the azimuthal angles in each figure. Panels of azimuth angles of $\theta = 40^\circ, 60^\circ, 80^\circ, 100^\circ, 120^\circ$, and 140° in figure 7 are in exactly the opposite directions: $\theta = 220^\circ, 240^\circ, 260^\circ, 280^\circ, 300^\circ$, and 320° in figure 8.

— Figure 7 —

— Figure 8 —

5. Structure of the Molecular Disk

5.1. Radial Distribution

Figure 9 shows a radial distribution of the surface density averaged azimuthally over the 1 kpc-width radius when the constant conversion factor was adopted. For a comparison, figure 9 also shows radial distributions calculated by Bronfman et al. (1988) and Grabelsky et al. (1987). The radius is reduced by factor of 8/10 because of difference in the adopted Galactic constant. Moreover, we adopted the conversion factor of 1.8×10^{20} although Bronfman et al. (1988) and Grabelsky et al. (1987) used X of 2.8×10^{20} . Hence, we reduced the surface density by factor of 1.8/2.8. The data from Bronfman et al. (1988) is a mean value of the northern and southern data. Filled squares, open circles, and open triangles denote the data from this study, Bronfman et al. (1988) and Grabelsky et al. (1987), respectively. The surface density decreases from $26.7 M_\odot \text{ pc}^{-2}$ to $0.3 M_\odot \text{ pc}^{-2}$ with the Galactocentric distance. Our result is almost consistent with Bronfman et al. (1988) and Grabelsky et al. (1987). The plotted values are given in table 1.

Radial distributions of the molecular gas in spiral galaxies are often expressed with exponential functions (Young et al. 1995). However, this figure shows that the radial profile is not expressed by an exponential function. The surface density is quite high at the Galactic center and near the 4 kpc radius, which is in response to the central condensation and Four-kpc ring found in the face-on map. The Galaxy is known to have a bar in the central region (e.g., Nakada et al. 1991). These double peaks are thought to relate to the barred structure (e.g., Nakai 1992).

— Table 1 —

— Figure 9 —

We also show the radial distribution of the molecular gas density at the midplane in figure 10. Radial distributions derived by Bronfman et al. (1988) and Grabelsky et al. (1987) are plotted for a comparison. The radius is reduced by factor of 8/10, and the density is multiplied by $(1.8/2.8) \times (10/8)^2$ because of the difference in the adopted Galactic constant and the conversion factor. Filled squares, open circles, and open triangles denote the data from this study, Bronfman et al. (1988) and Grabelsky et al. (1987), respectively. The radial distribution is similar to that of the surface density. The density decreases from 8.73 cm^{-3} to 0.03 cm^{-3} with the Galactocentric

distance. Our result is almost consistent with Bronfman et al. (1988) and Grabelsky et al. (1987). The radial profile of this value is not expressed by an exponential function, either. The plotted values are given in table 1.

— Figure 10 —

5.2. Scale-height

Figure 3 shows that the FWHM of the molecular gas disk slightly increases from 48 pc to 160 pc with the Galactocentric radius in the radius range of 0–11 kpc. The scale-height is smaller than that of the H I disk. The plotted values are given in table 1.

5.3. Midplane Displacement

Figures 7 and 8 show that the midplane of the inner disk is slightly displaced from the Galactic plane, which is known as a midplane displacement, a tilted disk, or warped disk. The warping of the outer disk was clearly delineated by May et al. (1997).

Figure 11 shows the midplane displacement versus the azimuthal angle θ relative to the Galactic center for individual radii. The vertical axis denotes the distance between the midplane of the molecular disk and the plane of $b = 0^\circ$. We calculated the midplane displacement, z_m , by averaging z with the weight of density, $n(z)$,

$$z_m = \frac{\int z n(z) dz}{\int n(z) dz}. \quad (8)$$

The midplane displacement can be expressed with a sinusoidal function. Hence, the molecular gas disk can be considered as a collection of tilted rings. We fitted the following sinusoidal function to the obtained data,

$$z_m = z_0 + A \sin(\theta - \theta_0). \quad (9)$$

The fitting algorithm used in this paper is the nonlinear least-squares Marquardt-Levenberg algorithm used in a software gnuplot. The obtained parameters are given in table 2. Figure 12 shows that amplitude of the midplane displacement is nearly constant inside a radius of 10 kpc. However, the amplitude steeply increases beyond the radius of 10 kpc, where the H I warp is remarkable (Nakanishi & Sofue 2003).

Figure 13 shows loci of the maximum points of individual tilted rings. The solid and dashed lines denote the loci where the midplane is displaced upward and downward, respectively. The loci form leading spiral arms, which is consistent with the rules of the warp summarized by Briggs (1990), and which is interpreted as follows: The midplane displacement can be considered as a wave, called a bending wave (Binney & Tremaine 1987). Defining Ω and ν as the rotational and vertical frequencies, respectively, the pattern speed of the bending wave is expressed as $\Omega + \nu/m$ or $\Omega - \nu/m$ (m : integer). Since the first one denotes a fast propagating wave and a trailing arm, it disappears rapidly as a result of the winding process. On the other hand, the leading spiral component is long-lived.

— Table 2 —

5.4. Central Concentration

A highly concentrated molecular gas, which is called the central molecular zone (CMZ; Morris & Serabyn 1996), is seen at the Galactic center. The gaseous column density reaches $\gtrsim 25 M_{\odot} \text{ pc}^{-2}$ at the center when we adopt a conversion factor of $1.8 \times 10^{20} \text{ cm}^{-2} \text{ K}^{-1} \text{ km s}^{-1}$. Though it is plausible that abundant molecular gas is distributed near the Galactic center, the shape shown in this map is suspicious, because the non-circular motion is noticeable in the central region due to the central Galactic bar. Sawada et al. (2004) created a face-on view of the CMZ using the data from the CO ($J=1-0$) survey of the Galactic central region Bitran et al. (1997). Because they derived it using without using the kinematic distance, their map is more reliable. The molecular gas in the CMZ is elongated in the line-of-sight direction. This feature is thought to be associated with a central galactic bar.

5.5. Spiral Arms

5.5.1. Scutum-Crux Arm

Positions of the edges of the Scutum-Crux arm in the first and fourth quadrants are $l = 33^{\circ}$ and $l = 305^{\circ}$ (Georgelin and Georgelin 1976). In the direction of $l = 305^{\circ}$, an arm-like structure can be detected around $(R, \theta) \sim (7 \text{ kpc}, 250^{\circ})$, which corresponds to a part of the Scutum-Crux. In figure 14, a schematic tracer of the Scutum-Crux arm is presented by a logarithmic spiral arm starting at $(R, \theta) = (3.0 \text{ kpc}, 30^{\circ})$ with a pitch angle of 12° . The parameters of these logarithmic spiral arms used in figure 14 are given in table 3.

— Table 3 —

5.5.2. Sagittarius-Carina Arm

The Sagittarius-Carina arm is a famous arm located near the Sun and is known to arc in the first and fourth quadrants (e.g., Georgelin & Georgelin, 1976; Cohen et al. 1985; Dame et al. 1986; Grabelsky et al. 1987; Grabelsky et al. 1988; Clemens, 1988; Solomon & Rivolo, 1989). According to Georgelin and Georgelin (1976), apparent edges of this arm are $l = 50^{\circ}$ and $l = 283^{\circ}$. This arm can be traced by a logarithmic spiral arm with a pitch angle of 11° . In figure 14, a schematic tracer of the Sagittarius-Carina arm is presented by a logarithmic spiral arm starting at $(R, \theta) = (2.0 \text{ kpc}, 180^{\circ})$ with a pitch angle of 11° .

5.5.3. Perseus Arm

A clear spiral structure can be found to arc from $(R, \theta) \sim (7 \text{ kpc}, 90^{\circ})$ to $(R, \theta) \sim (11 \text{ kpc}, 170^{\circ})$. This spiral arm is the so-called Perseus arm. This arm goes by the Sun outside the Solar orbit. The shape of this arm in our map is consistent with the result of Clemens, Sanders, & Scoville (1988). A cross section of this arm is found at $R = 10 - 11 \text{ kpc}$ in the top panel of figure 7. This arm can be traced more clearly in $l - v$ diagram of Dame, Hartmann, & Thaddeus (2001) and is detected from $l \sim 55^{\circ}$ in the negative velocity to $l \sim 270^{\circ}$ in the positive velocity.

This arm traced in the molecular gas map is consistent with that detected in the H I map (Paper I). It is more prominent in the H I map. The pitch angle of this arm was estimated to be 15° . In figure 14, a schematic tracer of the Perseus arm is presented by a logarithmic spiral arm starting at $(R, \theta) =$

$(5.7 \text{ kpc}, 30^{\circ})$ with a pitch angle of 15° .

5.5.4. Norma-Outer Arm

At larger radius than the Perseus arm, the Outer arm can be traced from $(R, \theta) \sim (9 \text{ kpc}, 50^{\circ})$ to $(R, \theta) \sim (11 \text{ kpc}, 120^{\circ})$. The Outer arm can be seen also in the longitude-velocity diagram of the CO survey (Dame, Hartmann, & Thaddeus 2001). This arm appears in the Galactic longitude range of $30 \lesssim l \lesssim 90^{\circ}$. The Outer arm is also detected in the H I map similarly to the Perseus arm. This arm traced in the molecular gas map is also consistent with that detected in the H I map, and is more prominent in the H I map. This arm can be traced with a logarithmic spiral arm with the pitch angle of 15° .

The Outer arm can be found in the vertical sliced map (figure 8). The Outer arm is located at the radius of $R \sim 9 - 12 \text{ kpc}$ in the $\theta = 80^{\circ}, 120^{\circ}$, and 140° panels of figure 8. Particularly in the $\theta = 120^{\circ}$ and 140° panels, this arm is displaced from the Galactic plane due to warping.

The Norma arm is known to exist in the fourth quadrant (e.g., Georgelin & Georgelin, 1976). Georgelin and Georgelin (1976) stated that the apparent edge of this arm is $l = 327^{\circ}$. In the fourth quadrant of our H_2 gas map, there is an elongated lump with a high H_2 column density in the direction of $l = 327^{\circ}$, which corresponds to the Norma arm. Though Georgelin and Georgelin (1976) mentioned that the Norma arm is symmetrical to the Sagittarius-Carina arm, the Norma arm seems symmetrical to the Scutum-Crux arm rather than the Sagittarius-Carina arm.

These two spiral arms seem to be the same arm, assuming the pitch angles of these arms are 15° . Hence, we call these arms the Norma-Outer arm. There are other possibilities of connections of (i) the Norma and Perseus arms and (ii) the Scutum-Crux and Outer arms. However, the radius of the Perseus is expected to be too small to be connected to the Norma arm in the fourth quadrant. Similarly, the radius of the Scutum-Crux arm is too large to be connected to the Outer arm in the first quadrant. Therefore, the connection of the Norma and Outer arms seems most natural.

In figure 14, a schematic tracer of the Norma-Outer arm is presented by a logarithmic spiral arm starting at $(R, \theta) = (4.0 \text{ kpc}, 240^{\circ})$ with a pitch angle of 15° .

5.5.5. Comparison with arms identified from HII region data

In order to evaluate the validity of the spiral arm that we trace, we compare our result with Georgelin and Georgelin (1976). We overlay the spiral arms that Georgelin and Georgelin (1976) traced on our tracing spiral arms in figure 15. The sizes of spiral arms are changed so that the distance between the Galactic center and the Sun is the same. The Sagittarius-Carina, the Scutum-Crux, and the Norma arms that we trace are coincident with those traced by Georgelin and Georgelin (1976), although the radius of the Perseus arm is slightly different for $l \gtrsim 90^{\circ}$ in the cases of our result and Georgelin and Georgelin (1976).

5.6. Ring-like structure

In the first quadrant ($0^{\circ} \leq l \leq 90^{\circ}$) a ring-like feature is found at $R \sim 4 \text{ kpc}$, which corresponds to the ring-like structure found by Clemens, Sanders, & Scoville (1988). The difference in the scale of this structure is due to the adopted R_0 . Clemens, Sanders, & Scoville (1988) adopted $R_0 = 10 \text{ kpc}$, while we

adopted $R_0 = 8$ kpc. Hence, the scale of our map is 4/5 times as large as the map of Clemens, Sanders, & Scoville (1988). We call this structure the Four-kpc Ring instead of the Five-kpc ring in this paper.

The edge of the Four-kpc ring corresponds to $l = 30^\circ - 40^\circ$. This coincides with the edge of the Scutum-Crux arm. In addition, the Sagittarius-Carina arm seems to be merged into the Four-kpc Ring in the azimuthal range of $\theta \lesssim 120^\circ$. The Four-kpc ring may therefore be a complex of two spiral arms and remarkably enhanced as if it was a ring.

Bronfman et al. (1988) pointed out that the radial distribution of molecular gas is flatter in the south hemisphere than in the north, and that the density peak at $0.5R_0$ in the north broadens in the south into a plateau. This statement is consistent with our conclusion that two spiral arms in the south are merged in the north.

6. Possible Errors in our Molecular Gas Map

Since the molecular gas map we obtained in this study is based on several assumptions, we must note the systematic errors due to deviations from these assumptions.

First, we assumed that the Milky Way galaxy rotates absolutely circularly around the Galactic center. However, the gaseous motion deviates from circular motion due to the density wave or the central Galactic bar, believed to exist at the Galactic center. The isovelocity contours are typically distorted in 1 kpc according to observations of external galaxies. Uncertainties concerning the location of the gas are about 1 kpc.

Second, we used the model expressed by equation (3) to divide the mixture emission from near and far points. Though the resultant map can change due to the adopted function, the global feature is almost the same for any function as shown in Paper I.

Third, fitting method does not necessarily work. Typical residual is less than 20 – 30 % of midplane density (figure 2). However, residual becomes much larger near the Sun, which implies that the fitting method does not work well in this region.

Fourth, conversion factor also affects the resultant gaseous map. We tried to make 3-D maps using a constant conversion factor and a varying conversion factor with the Galactocentric distance. Outer structure is enhanced when we use the varying conversion factor.

7. SUMMARY

We constructed a three-dimensional molecular gas map of the Milky Way Galaxy using the new compilation data set of $^{12}\text{CO}(J=1-0)$ survey obtained with 1.2-m telescopes and the latest rotation curve, based on the kinematic-distance. We made molecular gas maps by adopting two types of conversion factor; one is constant, and the other varies with the Galactocentric distance. Global features are the same for both though the contrast is slightly different.

We present a new 3-D map of the molecular gas in this paper. The resultant maps confirm the following features of the Galactic molecular disk.

1. The radial distribution of the molecular gas surface density has double peaks at the center and at the radius of $0.5R_0$, which is a feature similar to barred spiral galaxies.
2. The FWHM of the molecular disk slightly increases from 48 pc to 160 pc with the Galactocentric distance within the radius range of 0–11 kpc.
3. There is a midplane displacement, whose amplitude is nearly constant inside the radius of 10 kpc, increasing beyond this radius. The ridges of midplane displacement form leading spiral arms.
4. Molecular gas arms corresponding to the Outer, the Perseus, the Sagittarius-Carina, the Scutum-Crux, and the Norma arms could be traced as logarithmic spiral arms with the pitch angle of $11^\circ - 15^\circ$. Supposing that the pitch angles of the spiral arms are within this range, the Norma can be identified as being the same as the Outer arm.

We are grateful to Dr. Thomas Dame et al. for providing us with their large CO survey data.

References

- Alvarez, H., May, J., & Bronfman, L. 1990, *ApJ*, 348, 495
 Arimoto, N., Sofue, Y., and Tsujimoto, T. 1996, *PASJ*, 48, 275
 Binney, J., & Tremaine, S. 1987, Princeton, NJ, Princeton University Press, 1987, 747 p.,
 Bitran, M., Alvarez, H., Bronfman, L., May, J., & Thaddeus, P. 1997, *A&AS*, 125, 99
 Bronfman, L., Cohen, R. S., Alvarez, H., May, J., & Thaddeus, P. 1988, *ApJ*, 324, 248
 Bronfman, L., Alvarez, H., Cohen, R. S., & Thaddeus, P. 1989, *ApJS*, 71, 481
 Briggs, F. H. 1990, *ApJ*, 352, 15
 Clemens, D. P. 1985, *ApJ*, 295, 422
 Clemens, D. P., Sanders, D. B., & Scoville, N. Z. 1988, *ApJ*, 327, 139
 Cohen, R. S., Grabelsky, D. A., May, J., Alvarez, H., Bronfman, L., & Thaddeus, P. 1985, *ApJL*, 290, L15
 Cohen, R. S., Dame, T. M., & Thaddeus, P. 1986, *ApJS*, 60, 695
 Dame, T. M., Elmegreen, B. G., Cohen, R. S., & Thaddeus, P. 1986, *ApJ*, 305, 892
 Dame, T. M. et al. 1987, *ApJ*, 322, 706
 Dame, T. M., Hartmann, D., & Thaddeus, P. 2001, *ApJ*, 547, 792
 Dehnen, W. and Binney, J. 1998, *MNRAS*, 294, 429
 Georgelin, Y. M., and Georgelin, Y. P. 1976, *A&A*, 49, 57
 Grabelsky, D. A., Cohen, R. S., Bronfman, L., Thaddeus, P., & May, J. 1987, *ApJ*, 315, 122
 Grabelsky, D. A., Cohen, R. S., Bronfman, L., & Thaddeus, P. 1988, *ApJ*, 331, 181
 Hunter, S. D. et al. 1997, *ApJ*, 481, 205
 May, J., Alvarez, H., & Bronfman, L. 1997, *A&A*, 327, 325
 Morris, M., & Serabyn, E. 1996, *ARA&A*, 34, 645
 Myers, P. C., Dame, T. M., Thaddeus, P., Cohen, R. S., Silverberg, R. F., Dwek, E., & Hauser, M. G. 1986, *ApJ*, 301, 398
 Nakada, Y., Onaka, T., Yamamura, I., Deguchi, S., Hashimoto, O., Izumiura, H., & Sekiguchi, K. 1991, *Nature*, 353, 140
 Nakai, N. 1992, *PASJ*, 44, L27
 Nakanishi, H. & Sofue, Y. 2003, *PASJ*, 55, 191
 Sanders, D. B., Clemens, D. P., Scoville, N. Z., & Solomon, P. M. 1986, *ApJS*, 60, 1

- Sawada, T., Hasegawa, T., Handa, T., & Cohen, R. J. 2004, MNRAS, 349, 1167
- Solomon, P. M., Rivolo, A. R., Barrett, J., & Yahil, A. 1987, ApJ, 319, 730
- Solomon, P. M. & Rivolo, A. R. 1989, ApJ, 339, 919
- Spitzer, L. J. 1942, ApJ, 95, 329
- Young, J. S., et al. 1995, ApJS, 98, 219

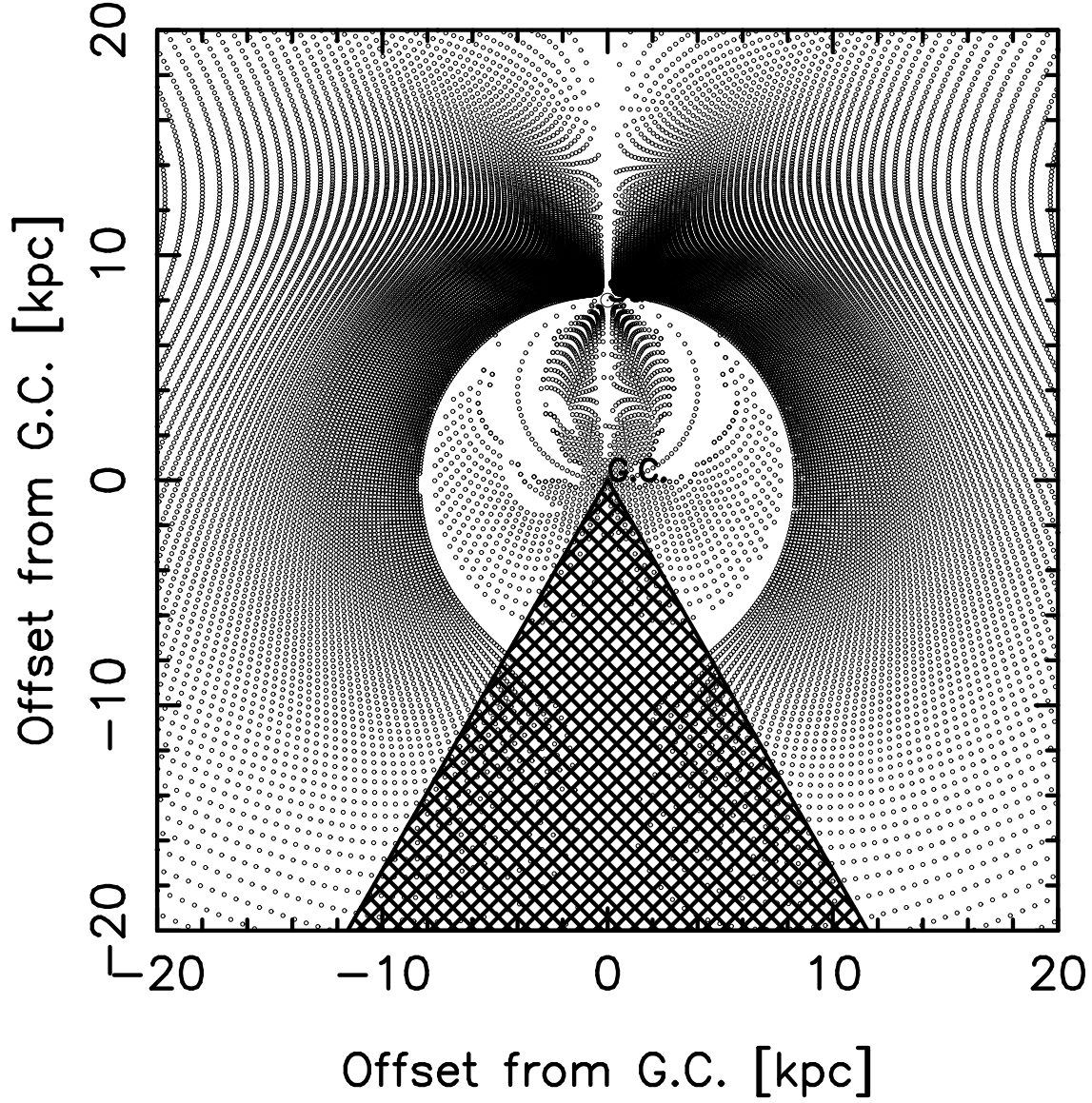


Fig. 1. Grid points where gas densities were calculated. The hashed area denotes a region where there are too few points to make a density map.

Table 1. Radial variations of parameters of the molecular disk

Radius (kpc)	Surface Density ($M_{\odot}\text{pc}^{-2}$)	Midplane Density (cm^{-3})	FWHM (pc)
0–1	26.7 ± 20.3	8.73 ± 6.91	48 ± 20
1–2	6.0 ± 5.4	1.28 ± 1.11	56 ± 18
2–3	3.5 ± 1.8	0.76 ± 0.42	68 ± 14
3–4	3.5 ± 1.6	0.75 ± 0.32	88 ± 24
4–5	4.6 ± 2.0	0.83 ± 0.38	78 ± 12
5–6	3.9 ± 2.0	0.66 ± 0.38	102 ± 10
6–7	2.8 ± 1.4	0.48 ± 0.27	84 ± 22
7–8	1.9 ± 1.0	0.26 ± 0.17	90 ± 30
8–9	0.9 ± 0.7	0.09 ± 0.07	186 ± 20
9–10	0.5 ± 0.4	0.05 ± 0.05	182 ± 20
10–11	0.3 ± 0.2	0.03 ± 0.03	160 ± 20

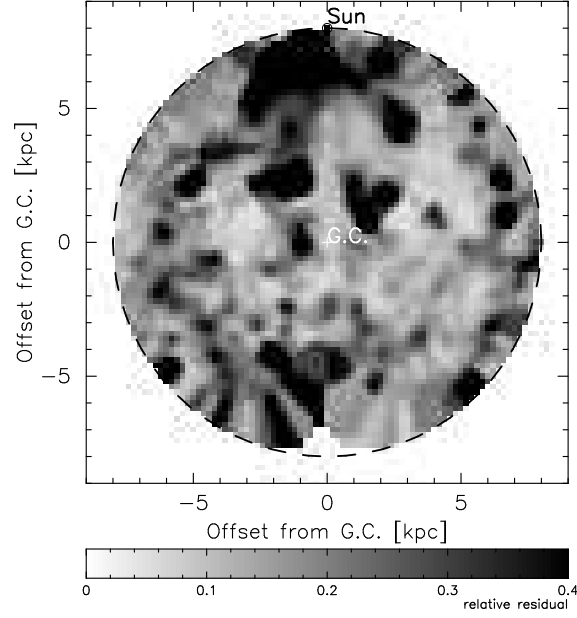


Fig. 2. Residual map. We here define the 'relative residual' to be a fraction of standard deviation of residuals between fitted model curves and observation data relative to the peaks of the observation data.

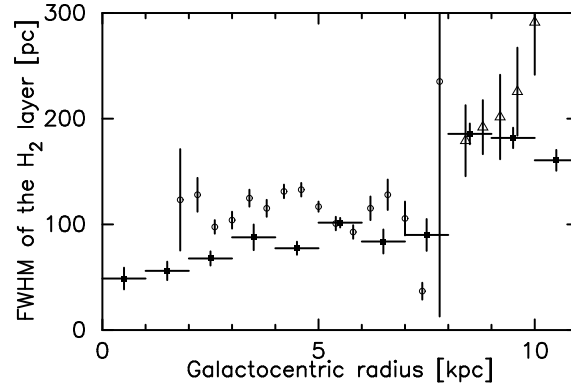


Fig. 3. FWHM of the H_2 gas layer versus the Galactocentric radius. Filled squares, open circles, and open triangles denote the data from this study, Bronfman et al. (1988) and Grabelsky et al. (1987), respectively.

Table 2. Fitted parameters of the midplane

Radius (kpc)	z_0 (pc)	A (pc)	θ_0 ($^\circ$)
0–1	5 ± 1	13 ± 1	292 ± 3
1–2	11 ± 1	36 ± 2	288 ± 4
2–3	-2 ± 4	22 ± 4	265 ± 15
3–4	-8 ± 5	12 ± 6	244 ± 32
4–5	2 ± 3	23 ± 4	277 ± 13
5–6	-12 ± 3	18 ± 5	190 ± 13
6–7	-6 ± 6	10 ± 9	193 ± 43
7–8	-9 ± 6	21 ± 9	133 ± 23
8–9	-27 ± 7	40 ± 9	109 ± 15
9–10	-49 ± 10	83 ± 12	76 ± 11
10–11	-26 ± 30	160 ± 25	85 ± 11

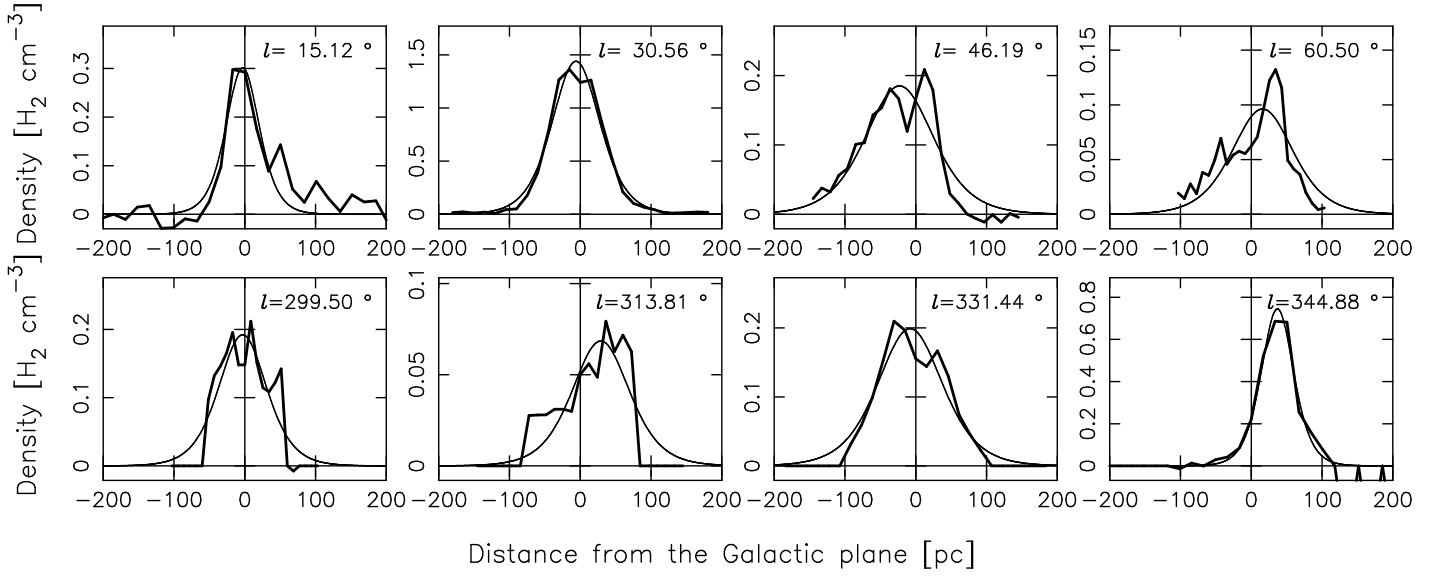


Fig. 4. Vertical distributions of the molecular gas. Horizontal and vertical axes denote height from the Galactic plane ($b = 0^\circ$) and H_2 density, respectively. Thick and thin lines indicate observation data and model curves, respectively.

Table 3. Parameters of schematic spiral arms

Name	PitchAngle ($^\circ$)	Beginning Point		Ending Point	
		(kpc)	($^\circ$)	(kpc)	($^\circ$)
Scutum-Crux	12	3.0	30	9.1	330
Sagittarius-Carina	11	2.0	180	10.5	310
Perseus	15	5.7	30	12.6	200
Norma-Outer	15	4.0	240	12.3	120

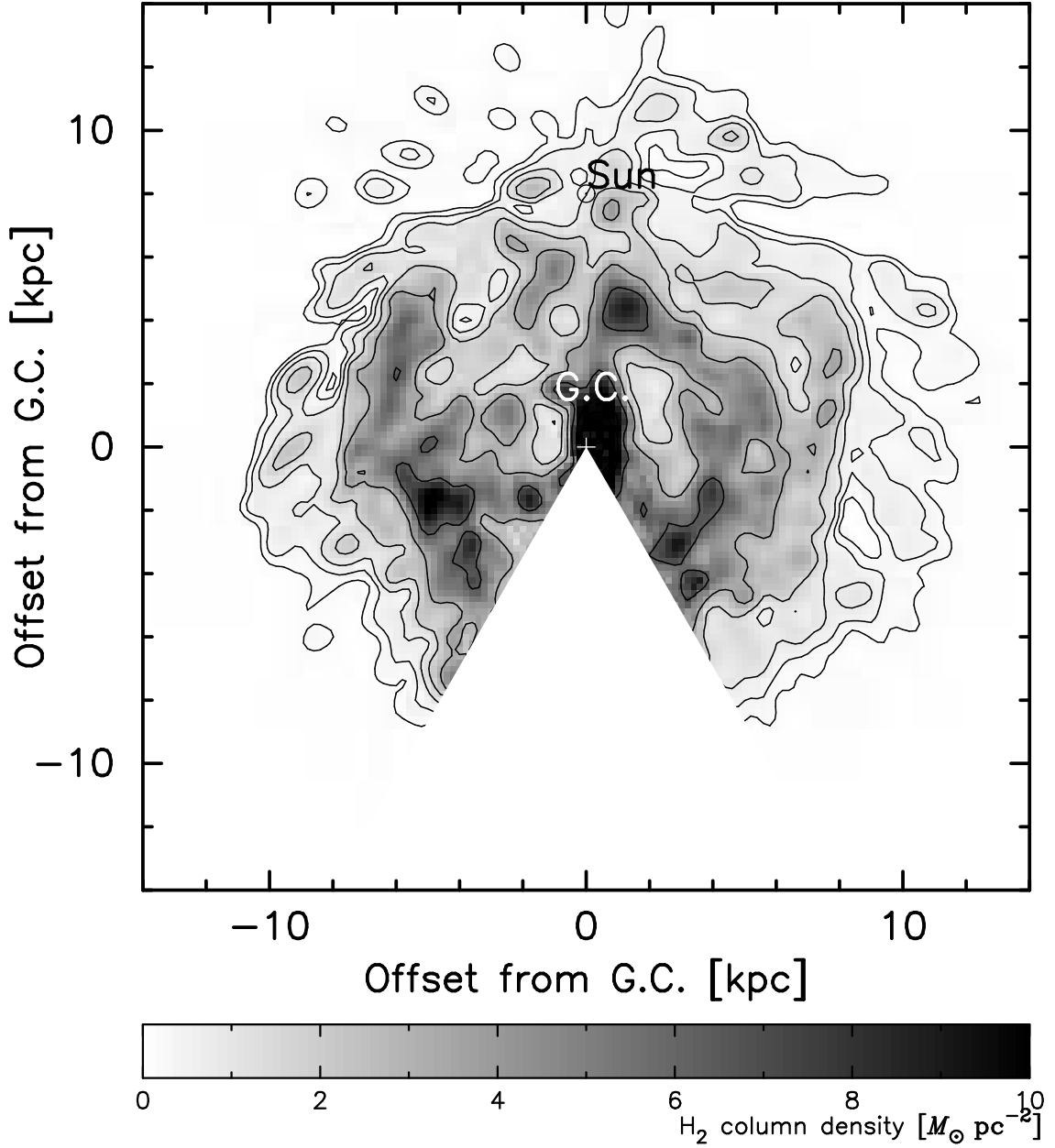


Fig. 5. Face-on molecular hydrogen map adopting the constant conversion factor of $X = 1.8 \times 10^{20}$ (Dame, Hartmann, & Thaddeus 2001). The contour levels are 0.2, 0.4, 0.8, 1.6, 3.2, 6.4, and $12.8 M_{\odot} \text{ pc}^{-2}$.

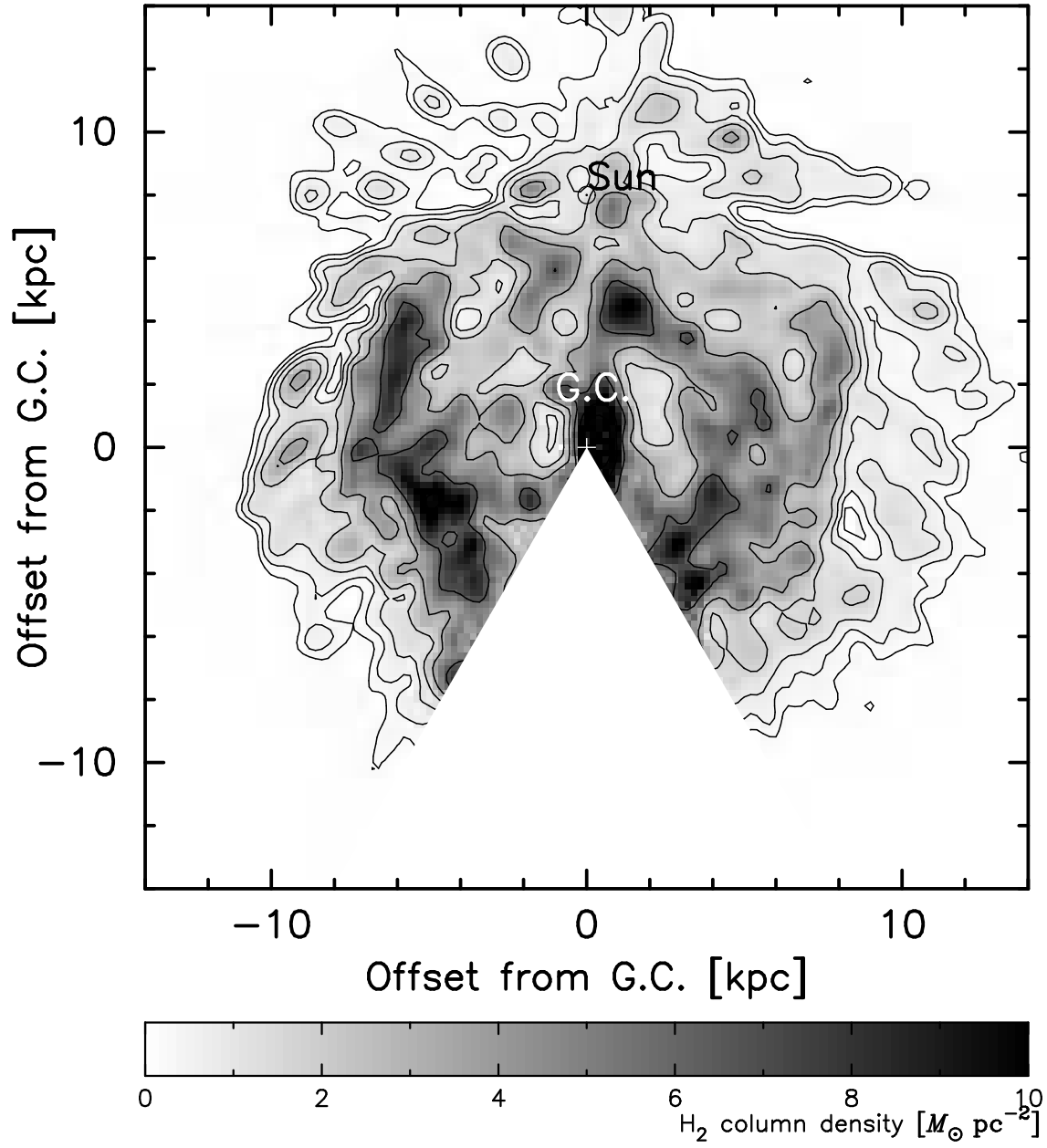


Fig. 6. Face-on molecular hydrogen map adopting the conversion factor X taken from Arimoto, Sofue, & Tsujimoto (1996), where X increases exponentially with the galactocentric distance. The contour levels are the same as those of figure 5; 0.2, 0.4, 0.8, 1.6, 3.2, 6.4, and $12.8 M_{\odot} \text{ pc}^{-2}$.

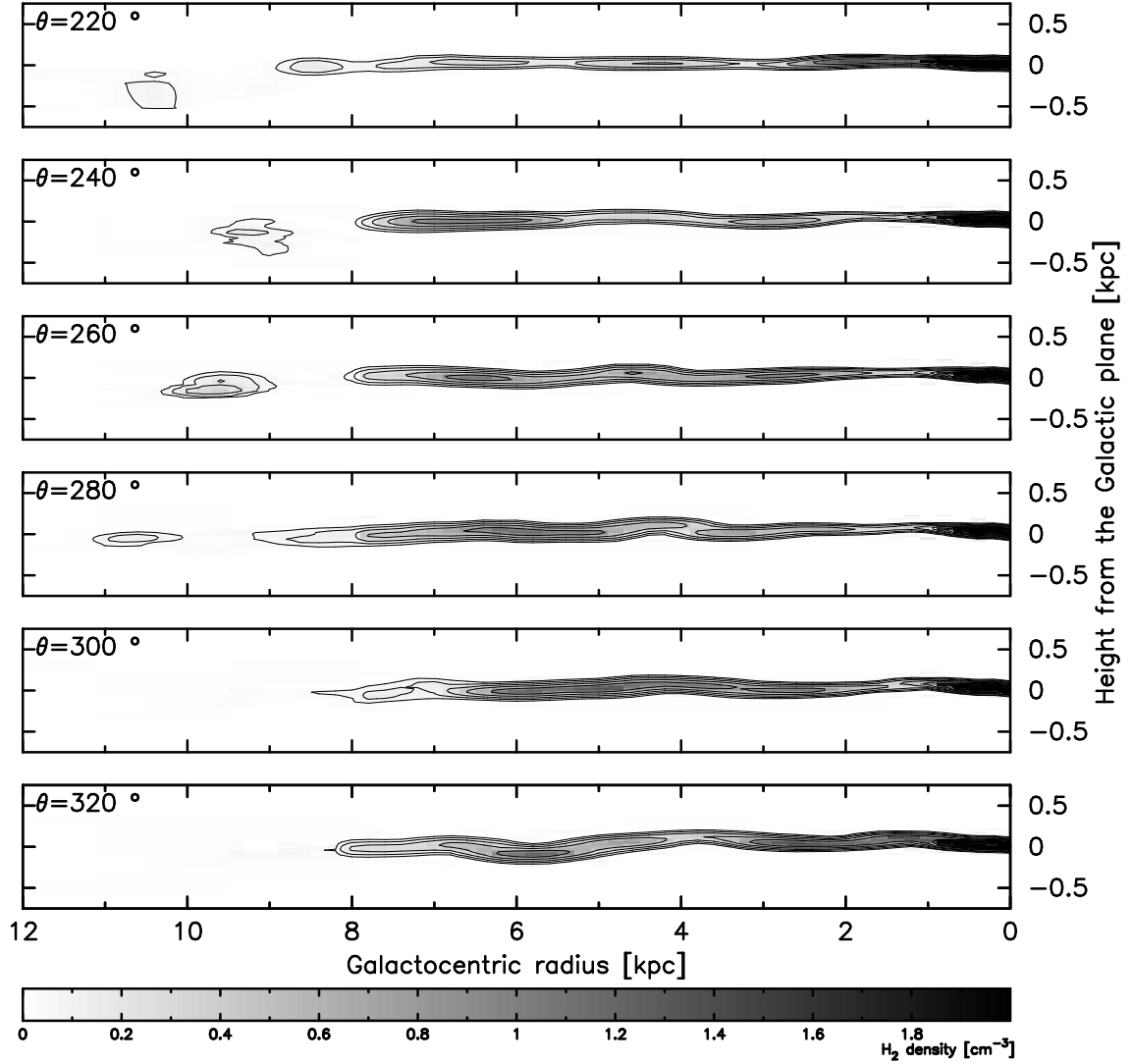


Fig. 7. Vertical cross-section maps. Each map shows the H_2 volume densities in a sheet through the Galactic center perpendicular to the Galactic plane. First plate: Individual panel shows sections through $\theta = 220^\circ$, $\theta = 240^\circ$, $\theta = 260^\circ$, $\theta = 280^\circ$, $\theta = 300^\circ$, and $\theta = 320^\circ$. The contours are drawn at levels of 0.05, 0.1, 0.2, 0.4, 0.8, 1.6, and $3.2 \text{ H}_2 \text{ cm}^{-3}$.

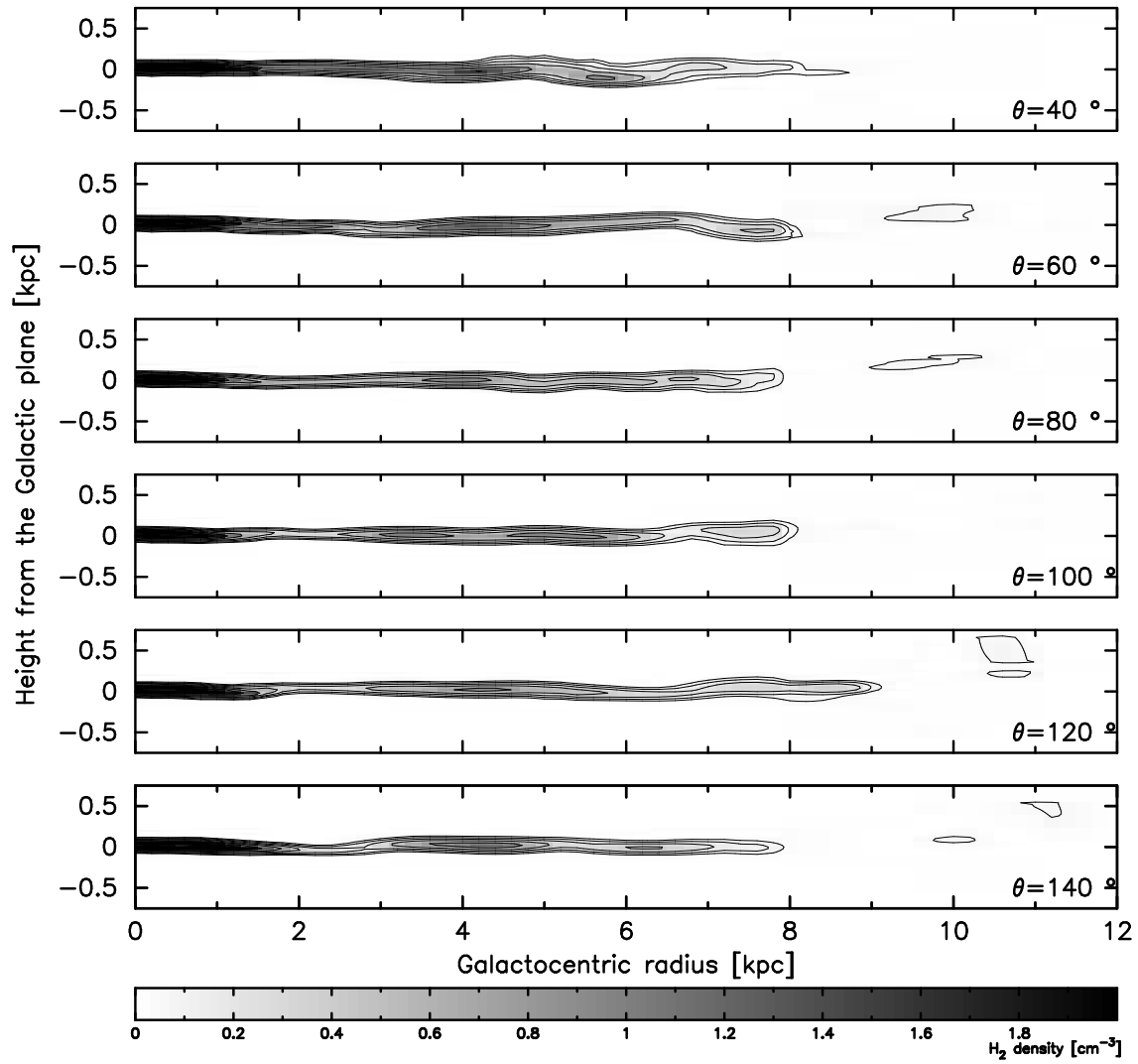


Fig. 8. Vertical cross-section maps. Each map shows the H_2 volume densities in a sheet through the Galactic center perpendicular to the Galactic plane. Individual panel shows sections through $\theta = 40^\circ$, $\theta = 60^\circ$, $\theta = 80^\circ$, $\theta = 100^\circ$, $\theta = 120^\circ$, and $\theta = 140^\circ$. The contours are drawn at levels of 0.05, 0.1, 0.2, 0.4, 0.8, 1.6, and $3.2 \text{ H}_2 \text{ cm}^{-3}$.

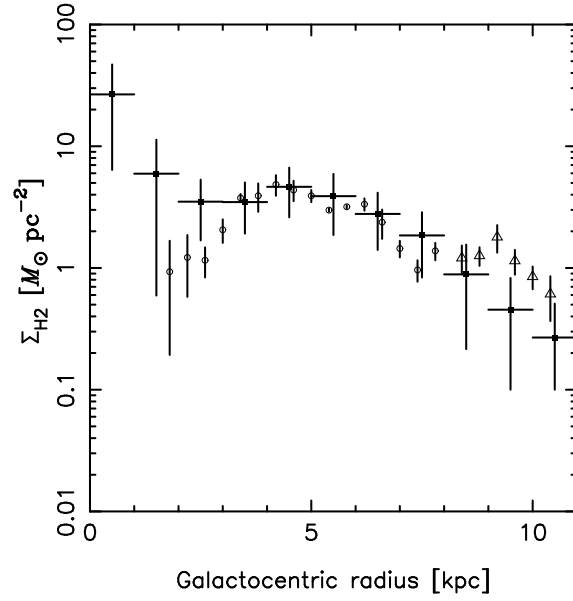


Fig. 9. Radial profiles of the H_2 gas surface density. The vertical axis is a logarithmic scale. Filled squares, open circles, and open triangles denote the data from this study, Bronfman et al. (1988) and Grabelsky et al. (1987), respectively.

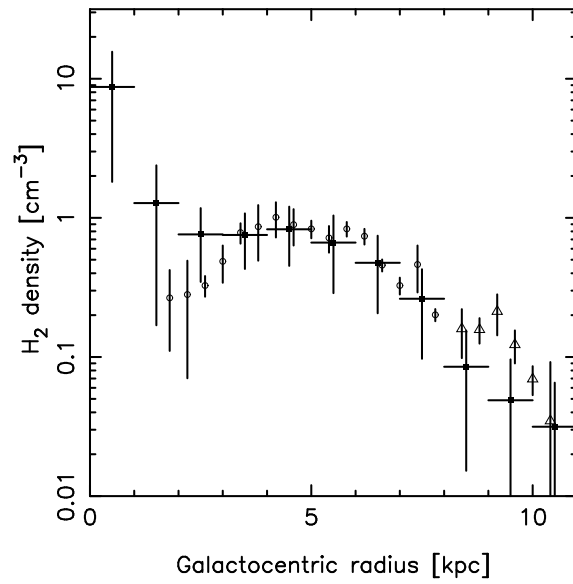


Fig. 10. Radial profiles of the H_2 gas density at the midplane. The vertical axis is a logarithmic scale. Filled squares, open circles, and open triangles denote the data from this study, Bronfman et al. (1988) and Grabelsky et al. (1987), respectively.

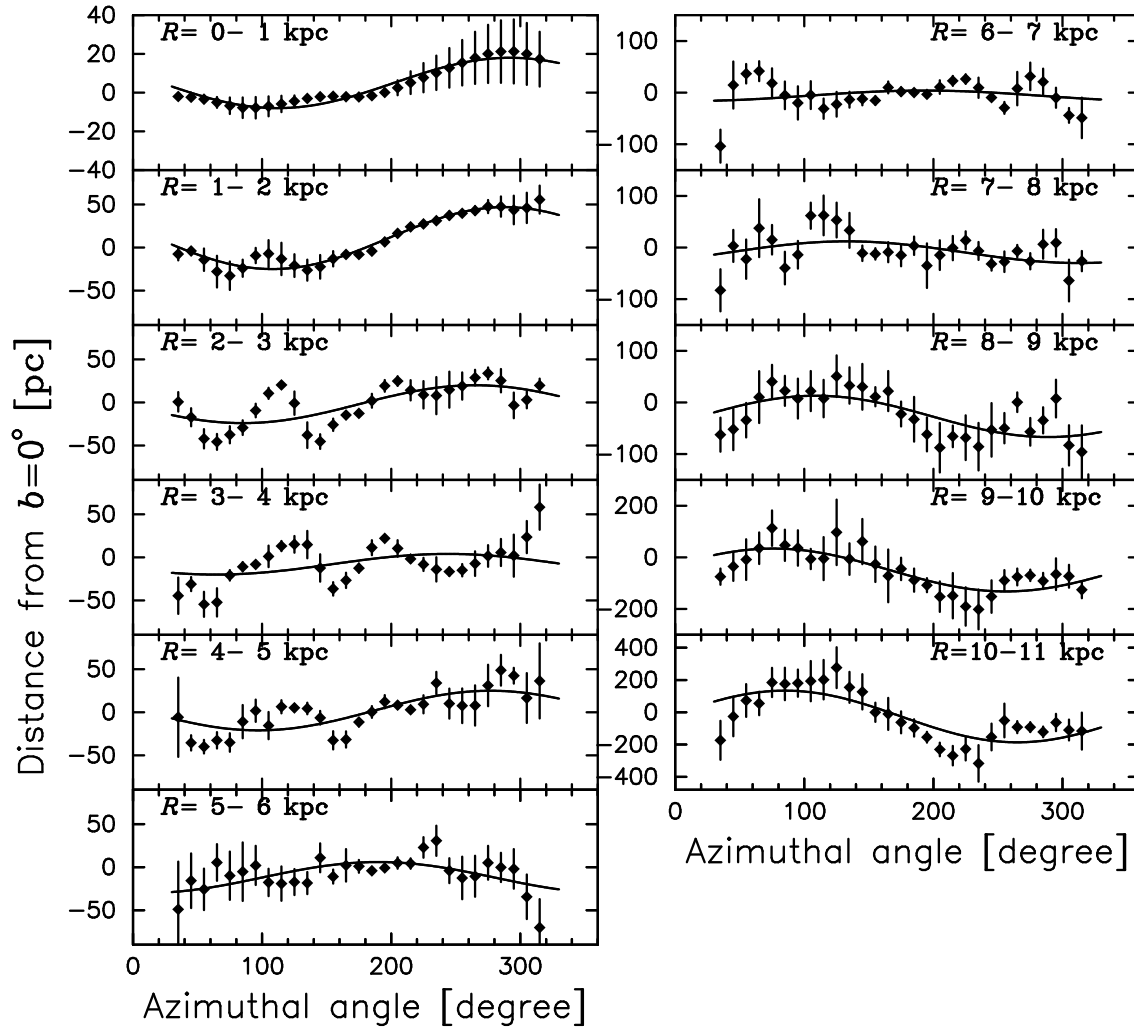


Fig. 11. Midplane displacements for individual radii. Horizontal and Vertical axes denote the azimuthal angle around the Galactic center and the distance from the plane of $b = 0^\circ$.

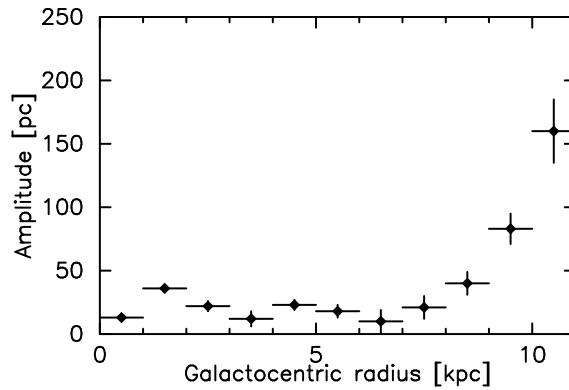


Fig. 12. The amplitude of the midplane displacement versus the Galactocentric distance.

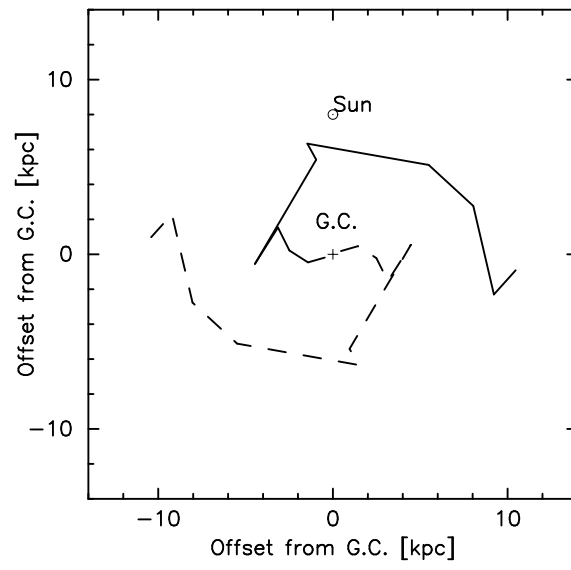


Fig. 13. Loci where the midplane displacements reach the maximum in the face-on view. The thick and dashed lines denote the loci where the midplane is displaced upward and downward, respectively.

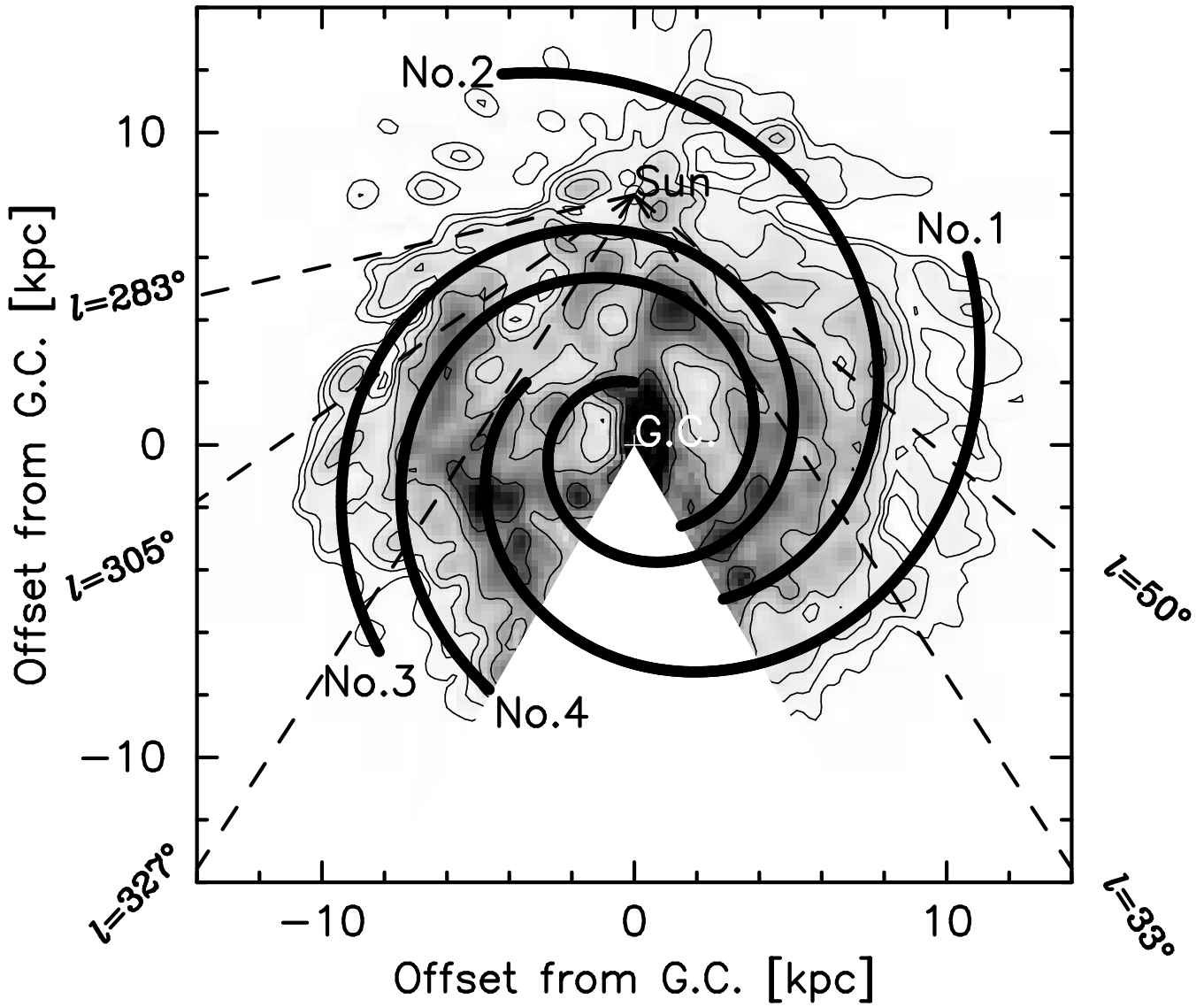


Fig. 14. Schematic tracers of H₂ gas arms superimposed on the obtained H₂ column density map; No.1: Norma-Outer arm; No.2: Perseus arm; No.3: Sagittarius-Carina arm; No.4: Scutum-Crux arm. The contour levels are the same as those of figure 5; 0.2, 0.4, 0.8, 1.6, 3.2, 6.4, and 12.8 $M_\odot \text{ pc}^{-2}$.

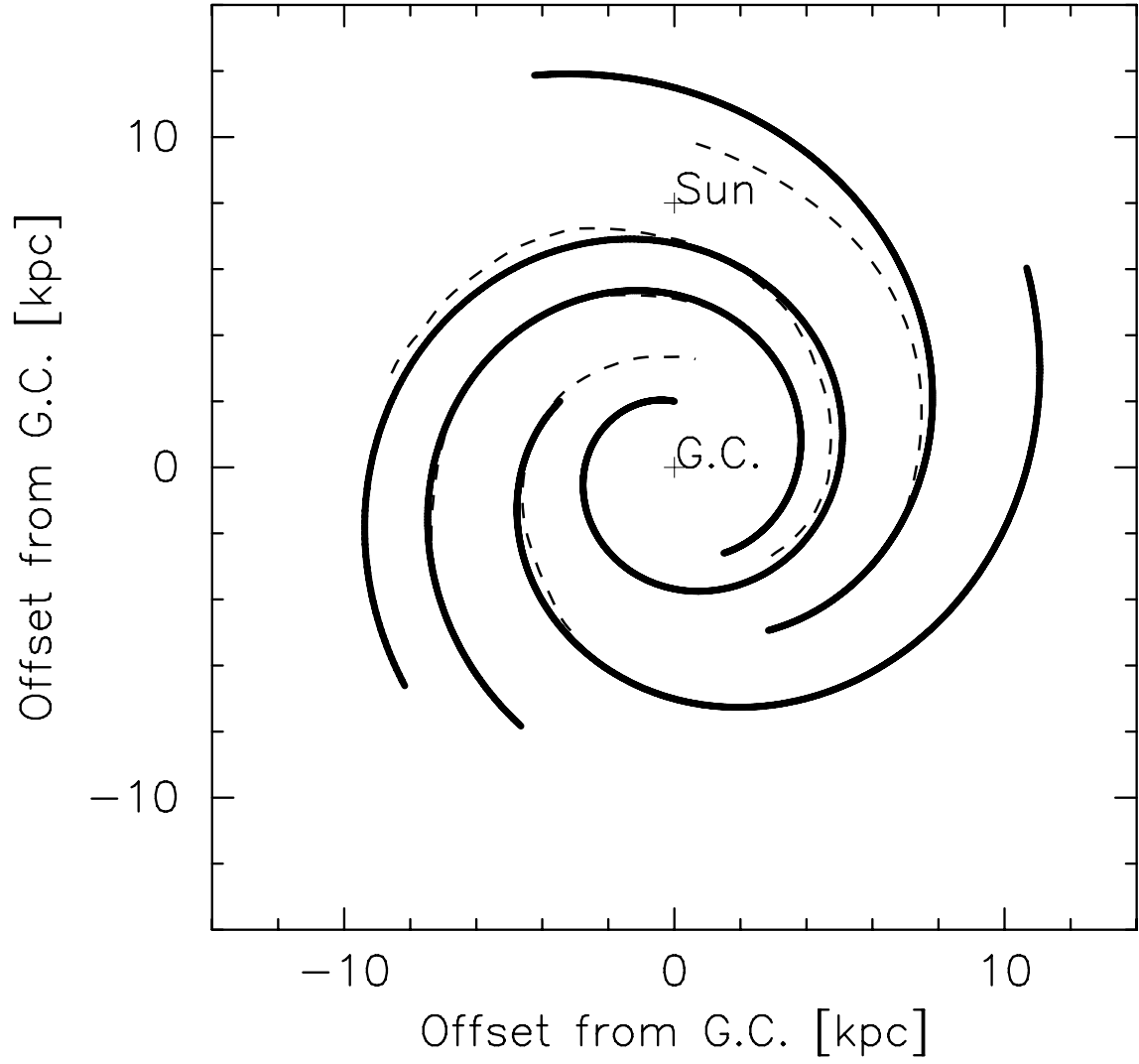


Fig. 15. Comparison of our result and spiral structure presented by Georgelin and Georgelin (1976). Thicker lines denote spiral arms which we traced. Thinner dashed lines denote spiral arms which Georgelin and Georgelin (1976) traced.